

RESEARCH ARTICLE

A freestanding, hierarchically porous poly(imine dioxime) membrane enabling selective gold recovery from e-waste with unprecedented capacity

Huaimeng Li^{1,2} | Mengxiang Ye^{1,2} | Zhen Fu¹ | Haimin Zhang^{1,2} |
 Guozhong Wang^{1,2} | Yunxia Zhang^{1,2} 

¹Key Laboratory of Materials Physics, Institute of Solid State Physics, Hefei Institutes of Physical Science, Chinese Academy of Sciences, Hefei, China

²University of Science and Technology of China, Hefei, China

Correspondence

Yunxia Zhang, Key Laboratory of Materials Physics, Institute of Solid State Physics, Hefei Institutes of Physical Science, Chinese Academy of Sciences, Hefei 230031, China.

Email: yxzhang@issp.ac.cn

Funding information

National Natural Science Foundation of China, Grant/Award Numbers: 51772299, 52173268; Presidential Foundation of Hefei Institutes of Physical Science, Chinese Academy of Sciences, Grant/Award Number: YZJZX202019

Abstract

The ever-growing depletion of precious metals in modern electronic industry necessitates unremitting exploitation of novel materials for gold recovery from e-waste. Herein, a freestanding poly(imine dioxime) (PIDO) membrane has been successfully fabricated for highly efficient recovery of gold from e-waste. The consummate integration of abundant binding sites and hierarchically porous architecture renders the resulting PIDO membrane with a record-breaking uptake capacity (9250 mg g⁻¹) toward gold, fast adsorption equilibrium time, as well as satisfactory regeneration and reusability. Furthermore, PIDO membrane is also well competent for selective gold recovery from waste central processing unit leachate with remarkable efficiency (>99%). Considering high recovery efficiency, outstanding selectivity, and simple/scalable production process, the proposed PIDO membrane will hold huge prospect in the sustainable recovery of gold from e-waste.

KEYWORDS

gold, poly(imine dioxime) membrane, recovery, regeneration, selective

1 | INTRODUCTION

As a double-edged sword, the accelerating development and innovation of electrical and electronic products affords a splendid life for the people; while their frequent replacement has led to the generation of mountains of waste electronic and electric equipment (WEEE). If being not managed scientifically, these WEEE will pose severe environmental burdens owing to a considerable amount of hazardous substances (e.g., halogenated organic pollutants and heavy metals).¹ On the other hand, most of electrical and electronic equipment are enriched in high-

value metals. For instance, CPUs contain ~280 g t⁻¹ of gold, which is much higher than that in a typical gold ore (3–30 g t⁻¹).² Hence, e-waste may be justifiably regarded as an invaluable secondary resource due to its high metal content. The overwhelming economic value of gold over other metals motivates the unremitting efforts associated with its efficient recovery from e-waste.³ Furthermore, the strict emission standards further necessitate the transformation of the obsoleted electronic devices into valuable wealth, that is, waste into treasure. With the non-renewable characteristics, limited supply and ever-increasing market demand of precious metal resources in

This is an open access article under the terms of the [Creative Commons Attribution](https://creativecommons.org/licenses/by/4.0/) License, which permits use, distribution and reproduction in any medium, provided the original work is properly cited.

© 2022 The Authors. *EcoMat* published by The Hong Kong Polytechnic University and John Wiley & Sons Australia, Ltd.

mind, tremendous attention has been attracted to gold recovery from e-waste in order to reduce the dependence on the existing mineral resources and address potential environmental risks as well as achieve the sustainable circular economy target.^{4,5}

To efficiently extract gold from e-waste, various recovery techniques have been developed, such as pyro- and hydro-metallurgical processes, solvent extraction, chemical precipitation, ion exchange, electrolysis, and adsorption.^{1,6} Among them, adsorption has been recognized as the most reliable means due to its easy operation, low cost, and high efficiency.⁶ Recently, numerous state-of-the-art adsorbents, for example, nitrogen-containing metal organic frameworks (MOFs),⁷ covalent organic frameworks (COFs),¹ porous aromatic frameworks (PAFs),⁶ and porous organic polymers (POPs),⁸ have been screened to capture gold species from complex solutions and made great breakthrough in lab tests benefiting from their inherently high porosity, large specific surface area, and abundant capture sites. Notwithstanding these encouraging progresses, unavoidable drawbacks associated with high cost, difficult separation due to the powdered or granular form, poor recyclability/regeneration, insufficient physiochemical stability under harsh acidic/basic conditions, and deficient applicability on a large scale, render them hardly meet the requirement for the practical gold recovery in real world. More importantly, the extracted gold by most adsorbents is in the existence of an ionic form and need further reduction to obtain its metallic form. Accordingly, it is urgent demand to explore novel adsorbents with reduction capability toward Au(III) and superior recovery performance, including high capture capacity, rapid kinetics, exceptional selectivity toward gold, facile recyclability, and excellent stability, to guarantee the sustainable supply of the precious metal resources.

To achieve the aforementioned goals, the common strategy is to graft specific functional groups (e.g., $-\text{NH}_2$, $-\text{SH}$, etc.) with strong coordination ability and remarkable selectivity toward gold onto the given adsorbents, so that the precious metal ions are inclined to accept electrons from the electron donor atoms (S and N) and form stable chelating bonds based on the hard and soft acids and bases (HSAB) theory.⁹ Thanks to excellent multidentate ligand with high nitrogen content of amidoxime, amidoxime-derived adsorbents have been designed in various types, such as polymeric fibers,¹⁰ porous polymers,¹¹ magnetic microspheres,¹² hydrogels,¹³ MOF,¹⁴ and exhibit excellent specificity and capacity for uranium sequestration. Beyond all doubt, amidoxime-based materials are also supposed to be the promising gold trapping agents based on the HSAB principle. Although well documented in the uranium recovery, amidoxime-based sorbents have less been investigated for the precious metal recovery. The existing

methods to fabricate amidoxime-based adsorbents are mainly involved in the following two categories. One is to firstly graft acrylonitrile monomer to some host materials (e.g., halloysite nanotubes,¹⁵ resin,¹⁶ biomass,¹⁷ polymer fibers,¹⁸ cellulose,¹² UiO-66-AO¹⁴) to form polyacrylonitrile (PAN) modified composites, followed by the subsequent chemical transformation of nitrile groups with hydroxylamine into amidoxime groups; while the expensive equipment is usually needed, especially for radiation-induced graft polymerization (RIGP) and atom transfer radical polymerization (ATRP) routes.^{13,18} The other is to fabricate poly(amidoxime) precursor solution beforehand and then mixed with polymer (e.g., poly(acrylamide),¹³ polyvinylidene fluoride¹⁹) membrane, porous substrates (e.g., montmorillonite,²⁰ graphene oxide²¹) or chemically cross-linked with glutaraldehyde/ Zn^{2+} to construct poly(amidoxime)-modified composites/porous networks.²² The two-/multi-step strategies mentioned above basically require complex operation processes and thus are unsuitable for the cost-effectively scalable fabrication. Additionally, these extra networks/supporting materials account for the partial weight of the overall adsorbents to some extent, resulting in the decreased proportion of effective coordination sites in per unit mass of adsorbent and thus exerting negative influence for the final extraction performance.

Considering the fact that the sequestration performance of gold is highly dependent on the accessibility and abundance of active sites and structural characteristics of adsorbents, it is reasonable to assume that designing a hierarchically porous amidoxime membrane excluding any foreign substance might significantly boost the resultant recovery capability toward gold, benefiting from fully exposed active amidoxime sites and favorable mass transfer of adsorbates. In sharp contrast to existing amidoxime-based adsorbents requiring the exogenous networks/supporting materials plus complex preparation procedures, herein, a free-standing, hierarchically porous PIDO membrane has been successfully fabricated via a facile, scalable fabrication technique for highly efficient recovery of gold from e-waste, in which PAN, commercially available, is first modified with hydroxylamine in organic solvent (DMF) to get PIDO solution via the covalent cross-linking, followed by subsequent self-assembly to form a hydrophilic PIDO membrane at the air/water interface. Structural characterizations demonstrate that the fabricated PIDO membrane features high specific surface area, outstanding hydrophilicity, ample amidoxime groups, interconnected porous network structure and good film-forming capability. The gold recovery performance of the proposed PIDO membrane is systematically evaluated by solution pH, contact time, initial solution concentration, and thermodynamic processes to optimize the gold recovery efficiency. Additionally, the

practical gold recovery potential of the PIDO membrane is assessed using waste CPU leachate. Finally, the gold recovery mechanism onto PIDO membrane is also explored by Fourier transform infrared spectroscopy (FT-IR), X-ray spectroscopy (XPS) measurements and density functional theory (DFT) calculations for the preferential binding behavior of gold with the N-sites of amidoxime.

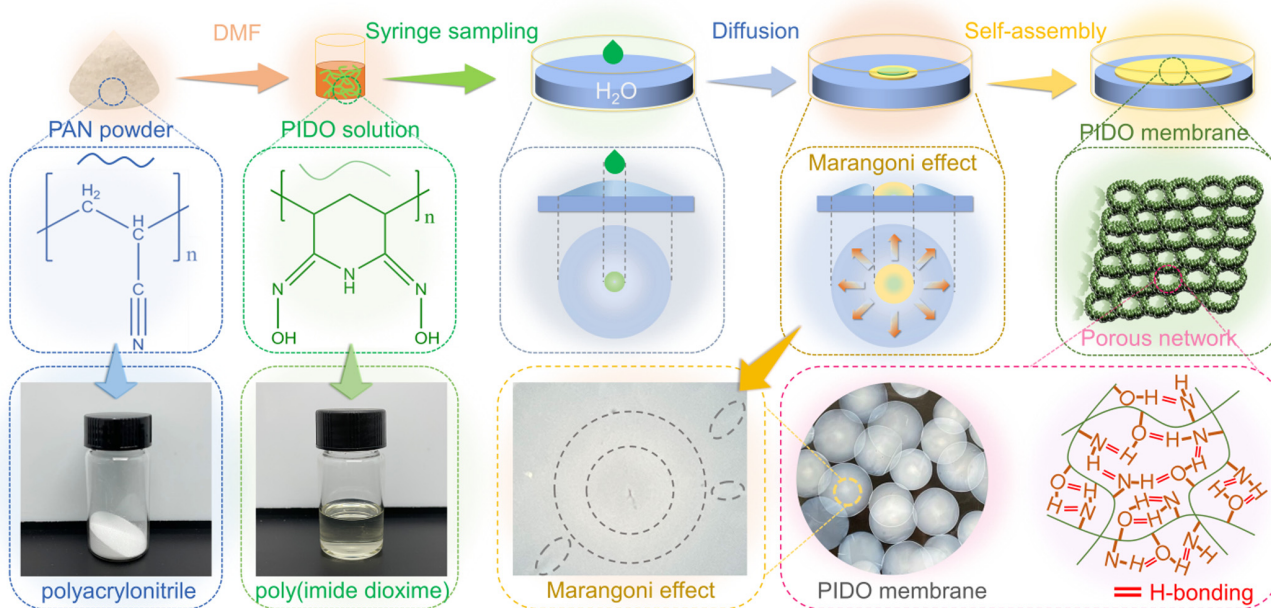
2 | RESULTS AND DISCUSSION

2.1 | Morphology and microstructural characterization of PIDO membrane

The fabrication process of PIDO membrane is schematically illustrated in Scheme 1. Firstly, the commercially available PAN powder can be well dissolved in organic solvent (DMF) to form a homogenous and transparent colorless solution. Upon the introduction of an alkaline solution of hydroxylamine hydrochloride, the amidoximated PIDO solution is generated after treatment at 80°C for 10 h based on straightforward nucleophilic addition reaction between PAN and hydroxylamine hydrochloride, in which nitrile groups of PAN are converted into amidoxime groups.²² Afterward, proper amount of the PIDO/DMF solution is continuously dropped dropwise with a syringe onto the water surface. With the diffusion and evaporation of DMF solvent, the capillary force between the PIDO microparticles increases via strong

intermolecular hydrogen bonds.²³ As a consequence, the PIDO microparticles dispersed in bulk solution can quickly spread in the direction parallel to the water surface and spontaneously assemble into a macroscopic, circle-like membrane at the air/water interface based on the Marangoni effect.^{23,24} It is noteworthy that the obvious rims at the periphery of the spreading film, diffusion stratification and folding phenomenon in the PIDO membrane are correlated with the evaporative instability of Marangoni effect.²⁵ In this way, numerous circular PIDO membranes with ultrathin thickness and macroscopic dimension can be massively produced under continuous flow using a peristaltic pump as the driving force in several seconds to minutes at room temperature, highlighting high reproducibility and easy scaled-up production of the method without any expensive equipment, which fully meet the sustainable requirement for the large-scale industrial application. Meanwhile, the macroscopic dimension of the fabricated PIDO membrane facilitates its convenient collection and subsequent recovery for reutilization.

The optical photograph in Figure 1A reveals intuitively the near-circular morphology of the as-obtained membrane with an average diameter of about 1 cm. Scanning electron microscopy (SEM) is utilized to identify the microstructural characteristics of the fabricated membrane. From Figure 1B, C, a highly porous 3D network is clearly found across the whole membrane surface, accompanied by homogenous void spaces with several micrometers confined in the



SCHEME 1 Schematic illustration for the fabrication process of poly(imine dioxime) (PIDO) membrane.

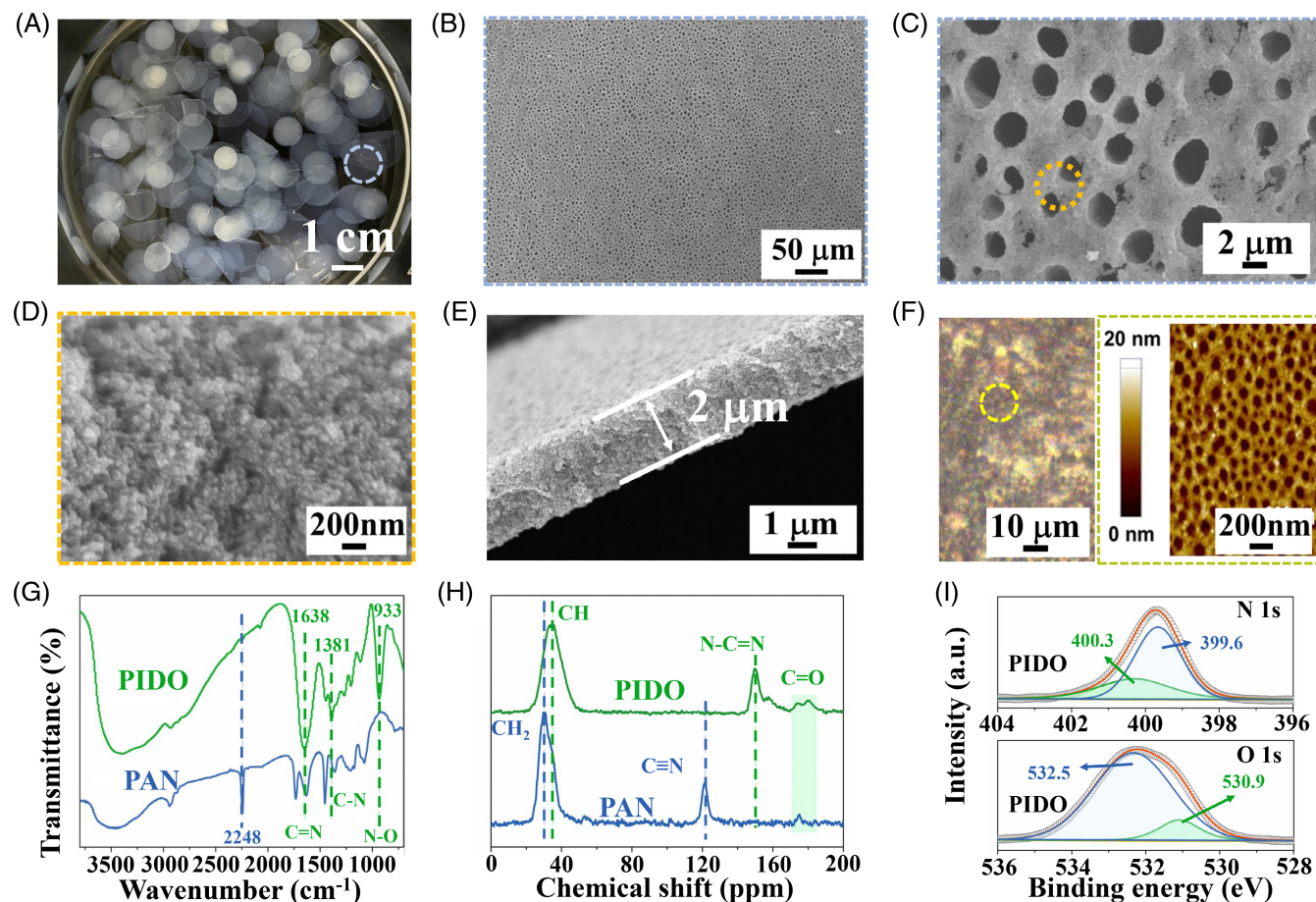


FIGURE 1 (A) Optical photograph of poly(imine dioxime) (PIDO) membrane. (B–D) Scanning electron microscopy (SEM) images of PIDO membrane under various magnifications. (E) cross-section SEM image of PIDO membrane. (F) Atomic force microscopy image of PIDO membrane. (G) Fourier transform infrared spectroscopy and (H) ^{13}C -NMR spectra of polyacrylonitrile and PIDO. (I) X-ray spectroscopy spectrum of PIDO membrane

as-obtained membrane over a large area. The magnified SEM image (Figure 1D) reveals that the channel wall of the membrane is surrounded by numerous closely packed PIDO sub-micrometer particles. Meanwhile, the thickness of the membrane is measured to be ca. 2 μm from the cross-sectional image (Figure 1E). The ultrathin characteristic of the fabricated membrane facilitates free diffusion of the adsorbed gold ions to the interior part. As reflected by atomic force microscopy (AFM) topographic image (Figure 1F), the PIDO membrane possesses a honeycomb structure with the rough surfaces, coinciding with the SEM results, in which the pore depth assembled by PIDO particles mainly centers at approximately 20 nm. Additionally, the effect of PIDO solution concentrations on the microstructure and morphology of the resulting membranes is further explored. As shown in Figure S1, the optimal concentration of PIDO solution is 5.0 wt% to obtain circular-like PIDO membranes. Both too low and too high concentration of PIDO solution are not favorable for the formation of regular membranes, which might be attributed to the

synergetic effect between surface tension and diffusion kinetics of solvents. The textural property and porosity of PIDO membranes are also checked by N_2 adsorption–desorption isotherm at 77 K (Figure S2). The specific surface area and pore volume of PIDO membrane are calculated to be 312 $\text{m}^2 \text{g}^{-1}$ and 0.20 $\text{cm}^3 \text{g}^{-1}$, respectively. The pore size distribution suggests the hierarchical porous structural characteristics of the fabricated membrane comprised of both mesopores and macropores, consistent with the SEM observations, which contributes to favorable mass transport and enhanced sorption kinetics. Such a high specific surface area of PIDO membrane not only contributes to full exposure of effective active sites but also ensures the efficient immigration of target metal ions/molecules along the interconnected open porous channels into the inner layer of the membrane, which plays a key role in improving its adsorption performance and accelerating adsorption kinetics. Energy dispersive X-ray spectroscopy (EDS) and elemental mapping analysis significantly confirm the uniform distribution of N, C and O elements in PIDO membrane

(Figure S3). The elemental analysis of the resulting PIDO membrane (Figure S4) reveals that the mass ratios of C, N, O, H elements are detected to be 40.8%, 31.5%, 20.9% and 6.8%, respectively, similar to the theoretical ratio of the cyclic imide dioxime, indicating sufficient oximation of PAN. The massive existence of well-dispersed amidoxime groups will render the resulting porous network membrane with complexing and reducing ability to transform the adsorbed AuCl_4^- into metallic gold. Additionally, the hydrophilicity of PIDO membrane is further verified by water contact angle tests. From Figure S5, the static water contact angle of PIDO membrane is measured to be 14.5° , indicative of its superhydrophilic character.²⁶ Such an excellent wettability and hydrophilicity coupled with 3D porous structure will facilitate ultrafast infiltration of water into the porous networks of PIDO and free diffusion of adsorbates in solution to the chelating sites on the surface and inner space of PIDO membrane. In addition, the stability of PIDO membrane at high temperature is further analyzed through the thermogravimetric measurement. As displayed in Figure S6, 2.1% and 33% of weight losses are found below 130 and 400°C), respectively, which are mainly caused by water evaporation and pyrolysis of oxygen-containing functional groups. In view of lower weight losses as compared to other amidoxime group composites,^{27,28} the fabricated PIDO membrane possesses superior thermal stability.

The formation of the resultant PIDO membrane is characterized via various techniques. Powder X-ray diffraction (XRD) is firstly used to reveal the crystal structure of the obtained samples. From Figure S7, the original PAN shows two strong characteristic peaks at $2\theta = 16.9^\circ$ and 29.6° , corresponding to the (100) and (110) reflections, respectively.²⁸ After amidoxime reaction, the characteristic diffraction peaks of PAN disappear; while a broad peak appears at 21.5° , indicative of the amorphous nature of the fabricated PIDO membrane.²⁸ FT-IR is carried out to verify the amidoxime transformation of nitrile. From Figure 1G, the nitrile group stretch ($\text{C}\equiv\text{N}$ stretch, 2248 cm^{-1}) from the pristine PAN disappears completely in the resulting membrane²⁹; while several characteristic signals associated with the amidoxime group that is, $\text{C}=\text{N}$ (1638 cm^{-1}), $\text{C}-\text{N}$ (1381 cm^{-1}), and $\text{N}-\text{O}$ (933 cm^{-1}) are clearly identified, suggesting the effective conversion of nitrile groups to cyclic imide dioxime and/or amidoxime groups.^{29,30} Considering the similar structures between amidoxime and imidedioxime, it is hardly to distinguish them from FT-IR spectra. Thus, the chemical structures of the as-obtained membrane are further elucidated by the solid-state ^{13}C nuclear magnetic resonance (NMR) spectra (Figure 1H). Two characteristic peaks are detected at 30 and 121 ppm for the raw material (PAN).²⁹ After amidoximation, the signal from the nitrile ($\text{C}\equiv\text{N}$) of PAN

completely disappears, while it occurs a red-shift for the peak at 30 ppm. Significantly, a strong signal appears at 150 ppm, accompanied by a weak peak at 160 ppm, which correspond to cyclic imide dioxime and open-chain amidoxime, respectively.²⁹ These NMR results indicate that the predominant products are cyclic imide dioxime rather than open-chain amidoxime during the amidoximation process.^{29,31} Considering the enhanced tridentate coordination capability of cyclic imide dioxime, the predominant formation of cyclic imide dioxime sites is highly expected to boost the final extraction performance toward gold. As reported, the hydroxyamidine generated by the reaction of hydroxylamine with nitrile is initially stabilized as a tautomer of amidoxime. Next, due to the nucleophilic nature of imine nitrogen, the hydroxyamidine can undergo intermolecular cyclization with adjacent nitrile groups, leading to the formation of imine dioxime. Note that a concomitant small peak associated with hydroxamic acid and amide groups is also detected in the carbonyl region of 170–180 ppm, consistent with the previous reports.^{31,32} The existence of amidoxime groups in the prepared porous network PIDO membranes is further verified by the XPS spectrum (Figure 1I). In the O 1s high-resolution XPS spectrum, the characteristic band at 532.5 eV can be attributed to $\text{HN}-\text{C}=\text{N}-\text{OH}$ from imine dioxime and/or amidoxime groups; while the appearance of carboxyl group at 530.9 eV might be originated from the part transformation of amidoxime groups in the alkaline treatment.^{29,30} Meanwhile, N 1s spectrum can be deconvoluted into characteristic peaks centered at 400.3 and 399.6 eV, corresponding to $\text{C}=\text{N}$ and $\text{N}-\text{H}$ groups, respectively.^{29,30} All these aforementioned analyses provide convincing evidence for complete transformation of $\text{C}\equiv\text{N}$ groups in the pristine PAN into $\text{C}=\text{N}$ in the resulting PIDO membrane.

2.2 | PIDO membrane enabling gold recovery

The abundant chelating coordination sites and potential reducing capability of the fabricated PIDO membrane prompts us to investigate its gold recovery performance in detail. Herein, various operating conditions are carried out to optimize the extraction efficiency toward precious metals. The influence of solution pH on the Au(III) recovery efficiency is initially analyzed by exposing the PIDO membrane to HAuCl_4 solution with a concentration of 100 mg L^{-1} under a wide range of pH conditions. As shown in Figure 2A, above 99% of the recovery rate of Au(III) is achieved between pH 1.0 and 4.0. A further pH increase from 5.0 to 7.0 results in a slight decrease of the recovery rate (e.g., 90.7% at pH 7.0), revealing that the

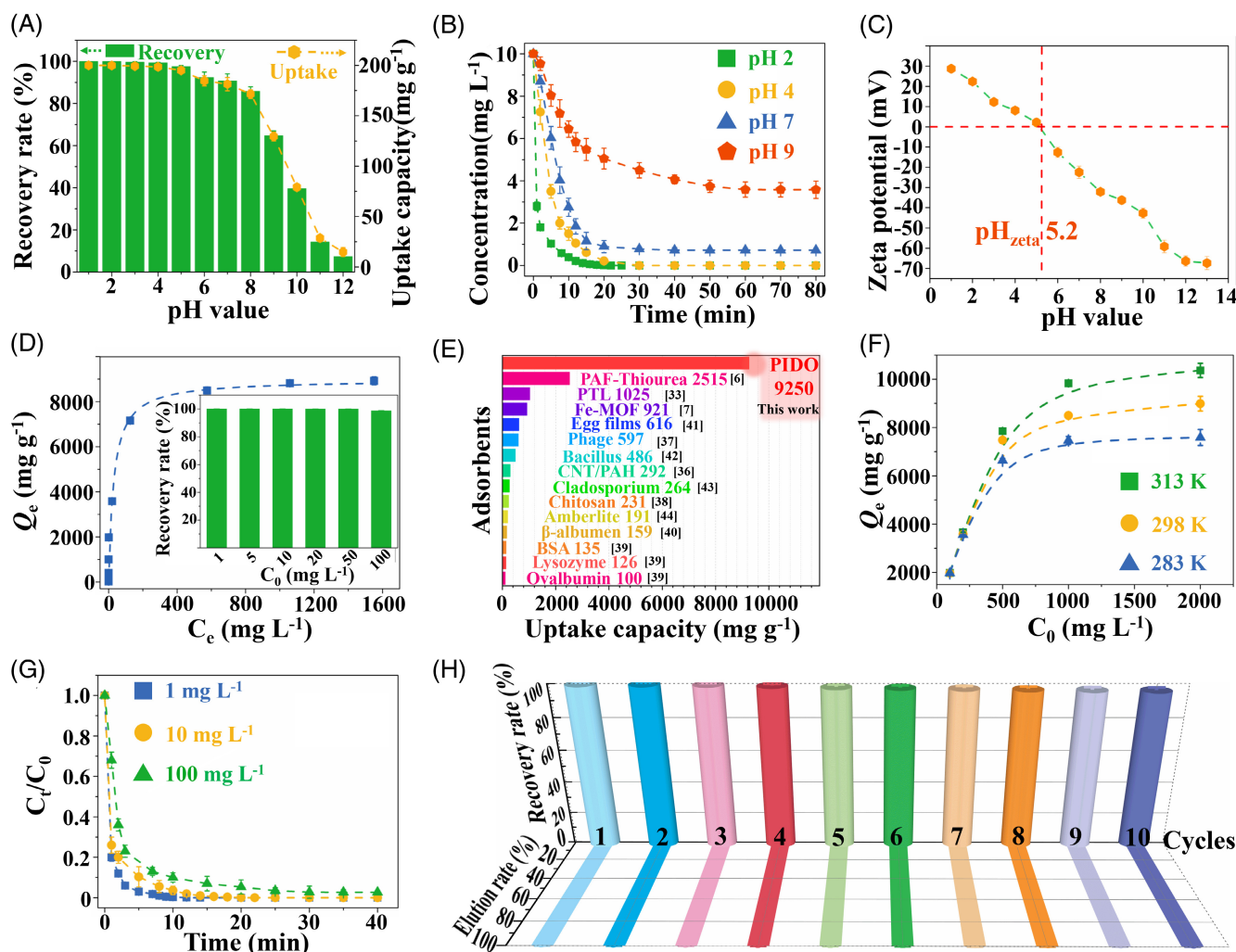


FIGURE 2 (A) Effect of initial pH on the adsorption capacities of Au(III) on PIDO membrane (0.05 g L⁻¹ of sorbent, 10 mg L⁻¹ initial concentration). (B) Adsorption kinetics of different initial pH of Au(III). (C) ζ -potential of the poly(imine dioxime) (PIDO) membrane at different pH values. (D) Adsorption isotherm of Au(III) on PIDO membrane (0.05 g L⁻¹ of sorbent, pH 3.0, 24 h for equilibrium, and a temperature of 25°C). (E) comparison of Au(III) maximum adsorption capacities on multifarious adsorbents. (F) The influence of temperature on adsorption capacities of Au(III) on PIDO membrane. (G) adsorption kinetics of different concentration of Au(III) (0.05 g L⁻¹ of sorbent, pH 3.0). (H) elution and reusability of the spent PIDO membrane

fabricated PIDO membrane is particularly suitable for extracting gold under acidic conditions. The phenomenon is actually advantageous for gold extraction from e-waste leachate since the e-waste is commonly digested in strong acid solutions. However, a sharp drop for gold uptake is found under basic pH conditions, accompanied by merely 7.8% of the recovery rate under pH 12.0, consistent with the previous literatures.^{1,6,33} Such a negligible gold uptake under the strong basic condition signifies the possible regeneration of the PIDO membrane loaded with gold via the simple basic treatment. Meanwhile, the influence of pH on adsorption kinetics is also studied. As shown in Figure 2B, at pH 2.0, the adsorption equilibrium can be achieved in 20 min, accompanied by 99% of Au(III) recovery efficiency. Further increasing solution

pH leads to reduced recovery rate and extended adsorption equilibrium time. Given the fact that solution pH affects the existing form of metal species and surface charge states on the membrane, the zeta potential values at varying pH are monitored to make out the reason behind the pH-dependent adsorption behavior. From Figure 2C, the isoelectric point of PIDO membrane is located at pH 5.2. At low pH (below 5.0), gold species mainly exist in the form of AuCl₄⁻ and AuCl₃(OH)⁻,³³ which tends to be electrostatically adsorbed by positively charged PIDO membrane, responsible for the observed high recovery efficiency of Au(III). When pH is higher than zero potential point, the surface of PIDO membrane becomes negatively charged due to the deprotonation of amino and hydroxyl groups; while gold species mainly

exist in the form of $\text{AuCl}(\text{OH})_3^-$ and $\text{Au}(\text{OH})_4^-$.³³ Accordingly, it occurs the electrostatic repulsion between gold ions and the membrane surface, yielding lower adsorption capacity for gold ions. Further, the negative charges on the PIDO surface increase with the increase of pH from 6.0 to 12.0. As a consequence, enhanced electrostatic repulsion for gold ions leads to the attenuation of recovery rate and the extension of adsorption equilibrium time.^{33,34} Considering the strongly acidic environment of the actual gold-containing leachate, pH 3.0 is chosen to carry out the subsequent gold recovery evaluation.

To determine the saturation adsorption capacity of Au(III) on PIDO membrane, the adsorption isotherms are obtained by immersing PIDO membranes (1.5 mg) into Au(III) solution (30 ml) with various initial concentrations at room temperature (Figure 2D). After stirring overnight to achieve the adsorption equilibrium, aliquots of the solutions are withdrawn and subjected to ICP analysis to determine the residual Au(III) concentration. It is evident that the equilibrium uptake capacity gradually increases with increasing Au(III) concentration in the range of 5–600 mg L⁻¹; while the curves level off when the initial concentration is higher than 1000 mg L⁻¹, indicating that the sorption has reached the maximum value since all the active sites are fully occupied. It is noteworthy that the extraction efficiencies of Au(III) are as high as almost 100% within the initial concentration range 1–50 mg L⁻¹ (the inset in Figure 2D). It should be noted that the spent PIDO membrane could be easily taken out from solutions after the treatment. The sorption data may be analyzed by the Langmuir adsorption isotherm and Freundlich adsorption isotherm model and the corresponding isotherm parameters along with regression coefficients (R^2) are summarized in Table S1. In view of higher correlation coefficient of the Langmuir model ($R^2 \geq 0.9999$) than the Freundlich isotherm equation ($R^2 = 0.9237$), the adsorption behavior of Au(III) on the surface of PIDO membrane is a uniform monolayer adsorption via complexation mechanism.³⁴ As usual, the Langmuir model can be defined more precisely by separation factor (R_L). As shown in Figure S8, the R_L values of the PIDO membrane are all less than 1 with the initial concentration of Au(III) ranging from 1 to 2000 mg L⁻¹, highlighting the favorable adsorption of Au(III) on the PIDO membrane.³⁵ From the adsorption isotherm, the maximum adsorption amount of Au(III) on PIDO membrane is calculated to be 9250 mg g⁻¹ based on the Langmuir model, very close to the experimental value of 8920 mg g⁻¹. To the best of our knowledge, the proposed PIDO membrane exhibits an ultrahigh adsorption capacity and remarkable extraction efficiency, outperforming all the other gold capture materials reported in the literatures to date (Figure 2E).^{6,7,33,36–44} Furthermore, the fabricated PIDO membrane can be extended for the recovery of other

precious metals, for example, Pt and Pd. As displayed in Figure S9a,c, the saturated adsorption capacity of PIDO membrane toward Pt(II) and Pd(IV) is as high as 3984 and 3103 mg g⁻¹, respectively. Meanwhile, the extracted platinum and palladium species are in metallic Pt and Pd form based on XRD characterizations (Figure S9b,d). Such a record-breaking adsorption capacity of PIDO membrane toward precious metals can be reasonably attributed to its high specific surface area, fully exposed and abundant binding sites (100% of amidoxime) due to no extra supporting materials or supplement.

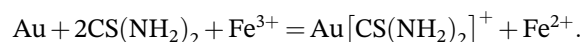
The adsorption process is further analyzed by the thermodynamic model. The dependent relationship between Au(III) adsorption capacity and operation temperature (T) is demonstrated in Figure 2F. Notably, the adsorption capacities increase with the increase of adsorption temperature from 283 to 313 K. For instance, the adsorption capacity increases from 7100 mg g⁻¹ at 283 K to 10 800 mg g⁻¹ at 313 K under 2000 mg L⁻¹ of the initial concentration, indicating that the elevated temperature is conducive to the adsorption of Au(III) on the surface of PIDO membrane due to the increase in surface activity and kinetic energy of the solute.³³ In order to study the spontaneity and feasibility of adsorption process, the thermodynamic parameters of Gibbs free energy (ΔG^0), entropy (ΔS^0) and enthalpy (ΔH^0) are deduced by Van't Hoff equation (Table S2). At lower initial Au(III) concentration (100 mg L⁻¹), ΔG^0 is negative at all the tested temperatures, indicating spontaneous adsorption of Au(III) on the surface of PIDO membrane (Figure S10a). With the increase of initial concentration, the adsorbed Au(III) occupies more active adsorption sites, resulting in the gradual increase of ΔG^0 .³³ Despite all this, ΔG^0 values are still negative even at high concentration (Figure S10b), confirming the feasibility and spontaneous nature of the Au(III) adsorption onto PIDO membrane.⁴⁵ Meanwhile, ΔH^0 and ΔS^0 are further derived from the intercept and slope of the plot of ΔG^0 versus T (Figure S1c). Note that the enthalpy ΔH^0 values are all positive, indicating that the adsorption of Au(III) on the PIDO surface is an endothermic process, consistent with the positive correlation of adsorption capacity with temperature. With increasing gold ion concentration, more gold species are immobilized on the membrane surface, resulting in the gradual weakening of thermal effect and the decrease of ΔH^0 . In addition to this, the entropy ΔS^0 values are positive in all cases, reflecting the increased randomness and chaos of the solid/solution interface during the adsorption process. That is, the adsorption of Au(III) on the PIDO membrane surface is an entropy-driven process. Similarly, the mobility of Au(III) on PIDO membrane surface is gradually restrained with the increase of Au(III) concentration, leading to the decrease of ΔS^0 .³⁴ To sum up, the adsorption of

Au(III) on PIDO membrane is an endothermic and spontaneous process.

Having identified the superior sorption capacity of gold, the recovery kinetic efficiency of PIDO membrane is also studied to further explore the adsorption pathways. The time-dependent recovery performance is performed with 50 mg of the PIDO membrane in 1 L Au(III) solution with varying initial concentrations, in which 3 ml aliquots are collected at increasing time intervals for the remaining concentration analysis in solution. From Figure 2G, it is apparent that the PIDO membrane exhibits extremely fast kinetics toward Au(III) in the initial 5 min and reached adsorption equilibrium within approximately 10 min with as high as 99% of extraction efficiency at an initial Au(III) concentration of 1 mg L⁻¹. Further increasing initial Au(III) concentrations from 10 to 100 mg L⁻¹, the adsorption time required to reach equilibrium is extended to 30 min, accompanied by the slightly reduced recovery efficiency (ca. 97.6% for 100 mg L⁻¹ of initial Au(III) solution). That is, the PIDO membrane possesses ultra-high adsorption kinetics toward Au(III) at both low and high initial concentrations. As well known, the adsorption kinetics is associated with the rate of mass transfer of Au(III) from the bulk solution phase to the binding sites on the surface or inside of the porous membrane. To obtain more information about the main rate-determining step, the time-dependent adsorption data are fitted by three kinetics models (Figure S11), namely, pseudo-first-order, pseudo-second-order, and intraparticle diffusion models, corresponding to a rate-determining step of pore diffusion, chemical adsorption, and intraparticle diffusion (including adsorbent surface adsorption and pore diffusion), respectively. Based on the linear regression analysis, the corresponding fitting kinetic parameters of the three adsorption kinetics models mentioned above are listed in Table S3. Apparently, compared with the pseudo-first-order (Figure S11a-c), the pseudo-second-order kinetic model is more suitable to the Au(III) adsorption process due to higher correlation coefficient ($R^2 \geq 0.9999$) (Figure S11d-f), suggesting that the dominant rate-determining step for the adsorption of Au(III) onto PIDO membrane is supposed to be chemical adsorption rather than the others.⁴⁶ Moreover, the intra-particle diffusion model also matches well with the adsorption data, indicating that adsorption of Au(III) on PIDO membrane is involved in a multistage process (Figure S11g-i). The initial stage is characterized by rapid adsorption of Au(III) on the outer surface of PIDO membrane. The second stage is mainly the diffusion process within particles. With Au(III) entering the interparticle pores, the diffusion resistance increases and the diffusion rate decreases. The third stage enters the final equilibrium stage, in which all available absorption sites in PIDO are completely

occupied, so the adsorption/desorption rate remains in equilibrium.³⁴ That is, the adsorption of Au(III) on the PIDO membrane involved in both the surface adsorption and its inner diffusion into the channels/pores. The observed fast adsorption kinetics of Au(III) is attributable to the unique 3D hierarchical porous structure and ultrathin thickness of PIDO membrane, reducing the ions diffusion barrier and ensuring full contact of Au(III) species with amidoxime binding sites inside the PIDO membrane.

Taking into account the cost-effectiveness of the extracting process in the practical application, the efficient desorption of gold and reusability of the PIDO membrane is particularly important. To this end, 10 successive extraction-desorption-reusability cycles of Au(III) on the fabricated PIDO membrane are carried out. First, 0.05 g L⁻¹ of PIDO membrane is immersed into Au(III) solution with the initial concentration of 10 mg L⁻¹. After Au(III) is extracted, the gold-loaded PIDO membrane is eluted using a mixed solution of thiourea (0.4 g L⁻¹) and Fe(NO₃)₃ (0.3 g L⁻¹) to restore the chelating active sites. Subsequently, the regenerated PIDO membrane is subjected to next cycle of Au(III) recovery under the identical conditions. The residual Au(III) concentration in solution is measured with ICP-MS and the desorption efficiencies are calculated. As shown in Figure 2H, the elution efficiency of gold is still over 98% after 10 rounds, confirming the effectiveness of the regeneration process and indicating the excellent recyclability of PIDO membrane. After desorption, the color of the PIDO membrane changes from golden brown to white, and the gold particles on the surface of the membrane are completely desorbed without affecting the surface morphology of the membrane (Figure S12a-c). SEM image reveals that the structural integrity of the PIDO membrane remained after the successive adsorption and desorption treatments (Figure S12d-f), guaranteeing the long-term stability and subsequent recyclability. From the corresponding EDS spectrum of the regenerated PIDO membrane (Figure S12g-i), the absence of discernable gold signals verifies the efficient desorption of gold from the PIDO membrane. The elution mechanism of gold can be described as follows⁴⁷:



Initially, Au⁰ immobilized on PIDO membrane can be oxidized into Au⁺ by Fe³⁺. Afterward, the generated Au⁺ ions tend to chelate with thiourea to generate stable complex (AuCS(NH₂)₂⁺) and are further released into the solution, rendering the exhausted PIDO membrane to be regenerated. Meanwhile, the resultant Fe²⁺ can effectively restore the reducing active sites on PIDO membrane to ensure the subsequent reusability. After assessing the effectiveness of gold desorption from PIDO membrane, the

recycling ability of this membrane is then confirmed by repeating the capture and elution procedure for 10 times. It is noteworthy that the regenerated PIDO membrane possesses over 98% of Au(III) recovery efficiency after 10 adsorption/elution cycles, indicative of its excellent reusability. By and large, the uptake capacity of gold on the regenerated PIDO membrane maintains unchanged throughout the 10 cycles. Such a satisfactory reusability together with excellent structural stability, superior recovery performance, and ease of scalable preparation, renders the fabricated PIDO membrane a sustainable adsorbent for gold recovery in the future practical applications.

2.3 | Recovery mechanism of Au(III) on PIDO membrane

To gain a deep insight into the interactions of Au(III) with PIDO Membrane, the samples before and after

Au(III) extraction are compared based on XRD, SEM, EDX, transmission electron microscopy (TEM), and FT-IR analyses. Upon immersing the white PIDO membrane into gold ions solution (with a concentration of 100 mg L^{-1}), the color of the membrane changes rapidly from white to golden yellow within 10 min by the naked eye (Figure 3A), indicating a possible spontaneous in situ redox reaction of Au(III) on the PIDO membrane surface accompanying the adsorption process.³³ In addition, the surface of the initial white PIDO membrane is observed to be covered with a layer of gold particles under the electron microscope (Figure 3B). In order to further confirm the above conclusion, XRD characterizations of PIDO membrane before and after Au(III) adsorption are carried out (Figure 3C). As expected, after Au(III) adsorption, several strong diffraction peaks are observed at 38.2° , 44.4° , 64.5° , 77.5° and 81.7° , in accordance with Au (111), (200), (220), (311) and (222) crystal planes of metallic gold (JCPDS No. 04-0784), respectively,⁷ revealing the

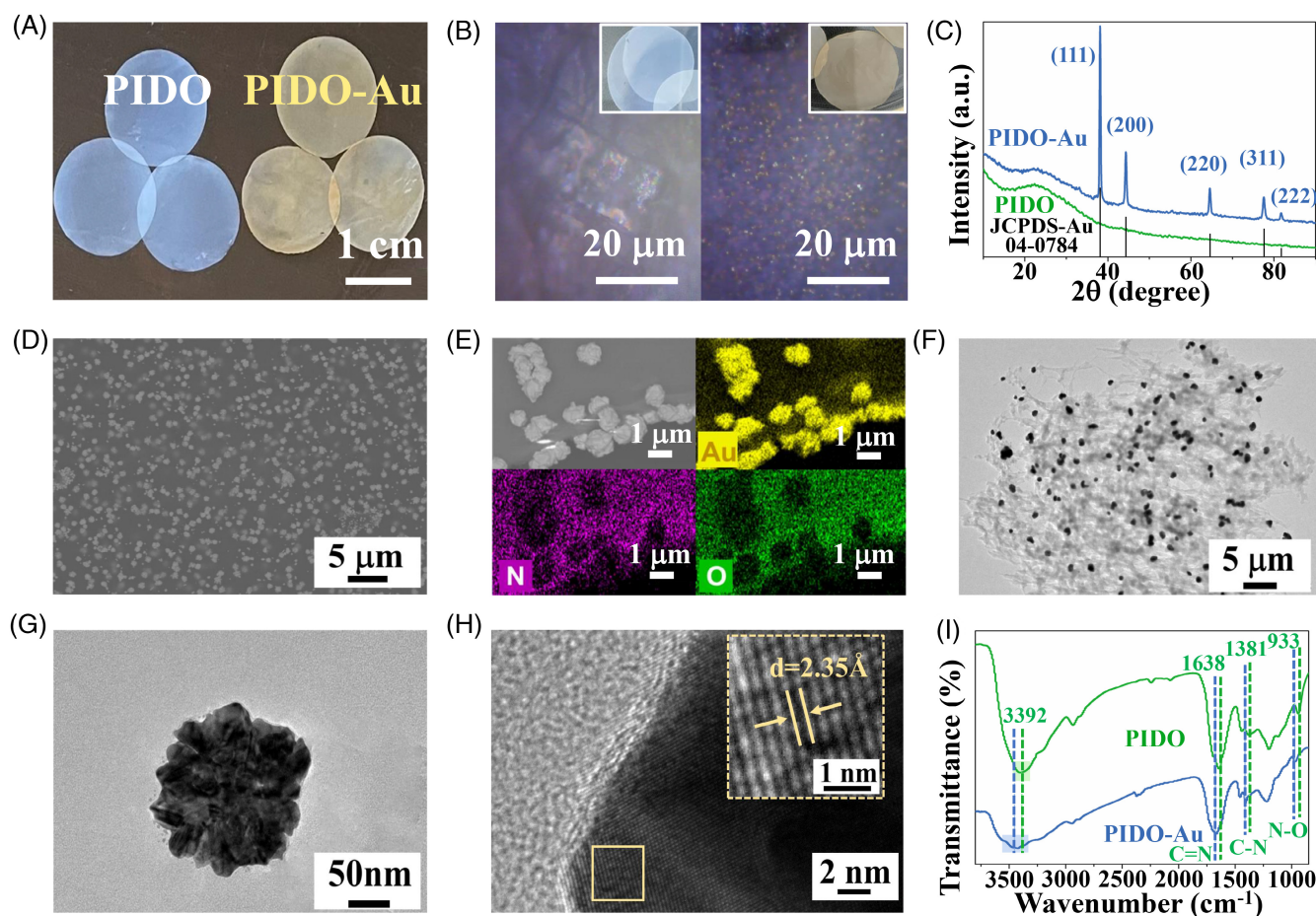


FIGURE 3 (A) Optical photograph of poly(imine dioxime) (PIDO) membrane before and after Au(III) uptake. (B) Microscope photographs of PIDO membrane before and after Au(III) uptake. (C) X-ray diffraction (XRD) spectra of PIDO membrane after Au(III) uptake. (D) Scanning electron microscopy image and (E) corresponding energy dispersive X-ray spectroscopy mappings of PIDO membrane after Au(III) uptake. (F–H) transmission electron microscopy image of PIDO membrane after Au(III) uptake. (I) Fourier transform infrared spectroscopy spectra of PIDO membrane after Au(III) uptake

excellent spontaneous reducing capability of the fabricated PIDO membrane and thus contributing to the recovery capacity for gold. Meanwhile, the broad peak around 21.5° in the post-sorption sample can be still detected with a similar intensity as compared to the pristine, indicating that the PIDO membrane loaded with gold retains its structural integrity during the Au(III) uptake and subsequent reduction process. This hypothesis is further evidenced by SEM and TEM images. The SEM image of the PIDO membrane after Au(III) adsorption is shown in Figure 3D, in which the typical sizes of the recovered gold particles anchored on the PIDO membrane range from dozens of nanometer to submicrometer scale. Besides, it is worth noting that EDS Elemental mapping analysis reveals gold particles are homogeneously distributed throughout the entire surface of the membrane (Figure 3E). Furthermore, TEM analysis also confirms the presence of gold nanoparticles on the membrane surface after Au(III) adsorption (Figure 3F,G). From the high resolution TEM (Figure 3H), the lattice distance of 2.35 \AA corresponds to the (111) lattice of metallic Au,⁴⁸ providing powerful evidence for the generation of metallic state Au and suggesting that the gold extraction on the PIDO membrane is based on a combined adsorption/reduction mechanism. Besides, FT-IR spectra of PIDO membrane before and after Au(III) extraction are also compared. As displayed in Figure 3I, after Au(III) capture, the decreased intensity and slight shifting to high wavelength are observed for C=N, C-N and N-O bands, suggesting the strong chelating action between amidoxime functional groups and Au(III).⁴⁹ Meanwhile, the peak around 3392 cm^{-1} , corresponding to stretching vibrations of -OH and -NH, becomes weaker and broader after Au(III) capture, revealing their participation in the complexing and reduction of Au(III).^{49,50} The above analyses fully verify that the PIDO membrane is capable of effectively extracting Au(III) species via strong chelating effect from aqueous media and further reducing them into metallic gold due to the immanent redox capability of imide dioxime groups, which is conducive to rebate the environmental pollution and energy consumption.

To seek further support for the synergistic adsorption and reductive mechanism of Au(III) on the PIDO membrane, the PIDO membranes before and after Au(III) capture are characterized by XPS. Compared with the survey XPS spectrum of the pristine PIDO membrane (Figure 4A), new peaks assigned to Au 4d and 4f evidently appear in the PIDO membrane after the Au(III) extraction. Meanwhile, the peaks at 84.3 and 87.9 eV are assigned to Au $4f_{7/2}$ and Au $4f_{5/2}$ (Figure 4B), respectively.⁶ Further, the valence state of the recovered gold is further explored by resolving the characteristic peak of

Au 4f. It is noteworthy that Au(0) (84.2 and 87.9 eV), Au(I) (85.2 and 88.9 eV) and Au(III) (86.7 and 90.7 eV) coexist in the PIDO membrane after the Au(III) extraction.^{1,6} Such different valence states of Au species on the PIDO membrane indicate the occurrence of a redox reaction between the sequestered Au(III) and amidoxime groups. Additionally, the area ratios of the three fitting peaks for Au(0), Au(I), and Au(III) are calculated to be 71.2%, 13.6%, and 15.2% respectively, in which the dominant Au(0) component indicates the strong reducing capability of the fabricated PIDO membrane toward Au(III). That is, Au(III) can be effectively reduced by the PIDO membrane into Au(I) and Au(0) during the Au(III) adsorption process due to ultrahigh content of N-containing amidoxime groups. The observation is consistent with the former literature reports that Au(III) can be reduced to Au(I) and Au(0) by the reductive nitrogen centers.^{1,6,33} To further identify the active sites of the PIDO membrane participated in coordination of Au(III) and subsequent reducing, the chemical states of N and O atoms before and after the interaction of the PIDO membrane with Au(III) adsorption are explored. As shown in Figure 4C, the intensity of N 1s decreases significantly and the binding energy increases notably after capturing Au(III), indicating that there is a strong interaction between Au(III) and N-containing functional groups.⁶ Additionally, the spectrum of N 1s can be deconvoluted into two characteristic peaks at 400.3 and 399.6 eV (Figure 4D), which are attributed to C=N and C-N-H, respectively. Note that both C=N and C-N-H groups shift to higher binding energy after binding with Au(III). The content of C=N basically remains unchanged; while the percentage of C-N-H decreases from 66.5% to 49.5% after capturing Au(III), indicated that imines in PIDO are involved in the chemical coordination and reduction of Au(III), resulting in the increased electron density of N atoms after gold capture.^{30,51} Further, a new peak associated with -NO₂ appears at 399.1 eV, caused by the oxidation of C-N-H during the Au(III) adsorption/reduction process. The aforementioned results fully demonstrate the coexistence of adsorption and reduction between the imines groups in PIDO and Au(III).^{52,53} Likewise, the spectrum of O 1s is further fitted into two bands at 532.3 eV and 531.1 eV (Figure 4E), corresponding to C=N-OH and COOH, respectively, in which the carboxyl group is originated from the part conversion of the amidoxime group during the alkaline treatment. After Au(III) capture, the peak associated with C=N-OH slightly shifts to lower binding energy with the decreased peak area from 86.8% to 74.2%; while the content of COOH group increases from 13.2% to 25.8%, indicating the strong chelation of the imide dioxime group with Au(III).^{29,30} Additionally, C 1s spectrum can be deconvoluted into three

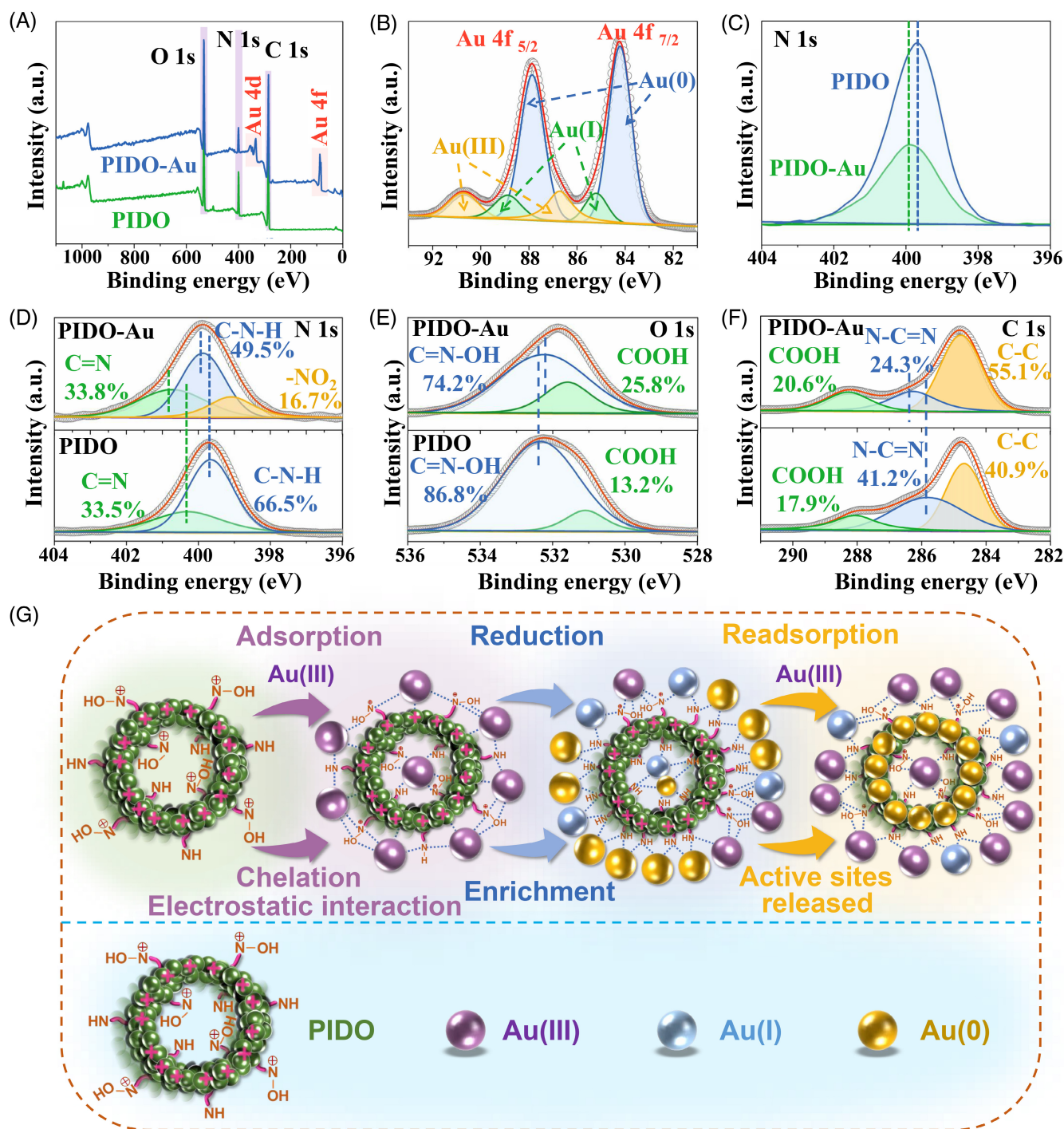


FIGURE 4 (A) X-ray spectroscopy (XPS) spectra of poly(imine dioxime) (PIDO) membrane before and after Au(III) uptake. (B) high-resolution XPS spectra of Au 4f. (C,D) N 1s, (E) O 1s and (F) C 1s XPS spectra of PIDO membrane after Au(III) uptake. (G) Schematic diagram of possible Au(III) adsorption and reduction mechanisms on PIDO membrane

characteristic peaks at 284.8, 285.8, and 287.9 eV (Figure 4F), corresponding to C–C, N–C=N and COOH, respectively.^{11,51} As compared to the bare PIDO, the peak assigned to N–C=N in gold-loaded PIDO shifts toward high binding energy and the corresponding content decrease from 41.2% to 24.3%, further indicating that

N–C=N group is involved in the adsorption/reduction of Au(III).^{51,54} Based on the above results, a possible recovery mechanism of Au(III) onto the PIDO membrane is proposed and presented in Figure 4G. First, Au(III) species are anchored on the PIDO membrane via the chelation of AuCl₄⁻ with the protonated amide and electrostatic

interactions in acidic media. Next, the captured Au(III) ions are reduced by the redox-active imide dioxime group to Au(I) and Au(0), giving rise to gold particles enriched in the skeleton of the PIDO porous network membrane. Finally, the occupied adsorption sites are restored to chelate additional Au(III) species, responsible for the resulting unprecedented recovery capacity of gold beyond expectation.

2.4 | Theoretical proof for Au binding on PIDO membrane

In an effort to gain comprehensive insight on the binding behavior of various metal ions on the PIDO surface, the density functional theory (DFT) calculations are carried out using Gaussian 16 with B3LYP. Considering the coexistence of the dominant cyclic imine dioxime and minor open-chain amidoxime in PIDO, the binding energies (E_{bind}) of various metal ions (e.g., Au(III), Pt(II) and Cu(II)) in both cyclic imine dioxime and amidoxime units are calculated. The E_{bind} values of Au, Pt and Cu are calculated by referring to Au(III), Pt(II) and Cu(II) ions in the respective AuCl_3 , PtCl_2 and CuCl_2 systems based on the sequential adsorption of metals by N- and O- sites in PIDO. Firstly, E_{bind} is calculated by removing chloride from AuCl_3 , PtCl_2 and CuCl_2 with the protonated amino and hydroxyl radicals of cyclic imine dioxime or amidoxime in acid condition to form HCl molecules. As shown in Figure 5A, -0.66 eV of binding energy is required for the cyclic imine dioxime unit to

capture one Au atom; while the corresponding binding energy greatly reduces to -2.93 eV upon the second Au atom continues to be sequestered, which indicates the gradual exothermic binding process and is consistent with the exothermic reaction in the aforementioned thermodynamic analysis. Such a stepwise reduction in binding energies is energetically conducive to efficient adsorption and agglomeration of Au. Likewise, cyclic imine dioxime strongly binds the single Pt atom at a lower binding energy of -1.27 eV, and more negative binding energy (-2.45 eV) is demanded to capture the second Pt atom. Evidently, both Pt and Au possess a similarly gradual exothermic binding process, thus providing a driving force for their adsorption and subsequent agglomeration. Although the initial binding energy of single Pt atom on the cyclic imine dioxime is lower than that of single Au atom, the capture of the second Au is more energetically favorable as compared to the second bound Pt, which coincides with the experimental capture capacity data (9250 mg g^{-1} for Au and 3984 mg g^{-1} for Pt). As for Cu, the binding energy of one Cu atom is 1.63 eV, indicating that the capture of Cu atom is hindered in terms of energy. Although the binding of the second Cu atom results in the declined binding energy (0.33 eV), the overall positive binding energy is still adverse to the capture of Cu.

Next, the adsorption mechanism of various metals on a small amount of amidoxime structure is also probed via DFT calculations. As demonstrated in Figure 5B, the stepwise binding energies of single Au atom and two Au atoms captured by amidoxime are -0.41 and -2.49 eV,

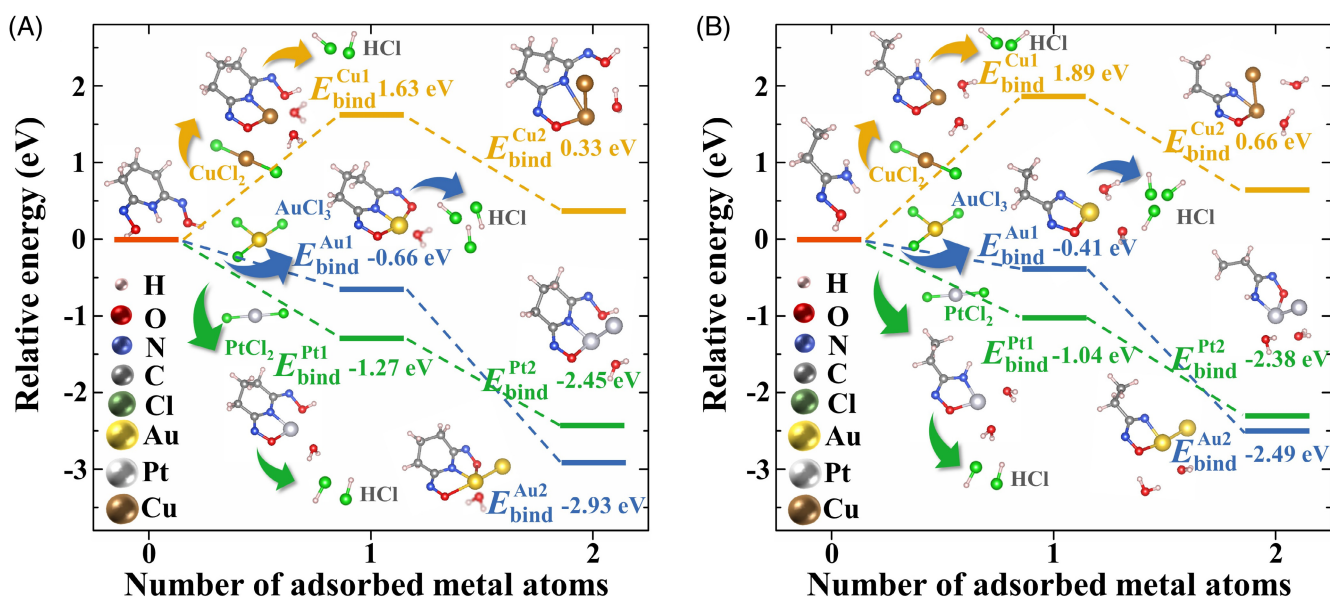


FIGURE 5 Density functional theory calculations for energy of binding (E_{bind}) changes in sequential adsorption in multinuclear adsorption of Au, Pt, and Cu on a model unit of cyclic imine dioxime (A) and amidoxime (B)

respectively. It is noteworthy that the binding capability of amidoxime toward Au is theoretically weaker than that of cyclic imine dioxime; while there exists efficient aggregation driving force for gradual exothermic action in the amidoxime structure. Additionally, there is an identical variation trend in the binding energies of one and two Pt atoms bound by the respective amidoxime and cyclic imine dioxime, accompanied by the negative overall binding energy, in which the exothermic effect during the binding process is responsible for favorable adsorption agglomeration of Pt, Au. For Cu, the binding energies of the first and the second Cu atom bound by amidoxime are 1.89 and 0.66 eV, respectively, indicating that it cannot occur the adsorption of Cu atom on amidoxime in terms of energy, consistent with the extremely low separation coefficient (K_d) due to the adverse adsorption of Cu on PIDO. These DFT theoretical calculations are well consistent with the former experimental observations, where the fabricated PIDO membrane can selectively recover Au from e-waste despite the existence of Cu with high content.

2.5 | Authentic gold recovery from waste CPUs

The efficient and selective extraction of precious metals from real e-waste sources containing various metals is

rather challenging. Encouraged by the comprehensive extraction experiments in Au(III) standard solution mentioned above, we further testify the feasibility of the PIDO membrane in the authentic extraction applicability of gold from e-waste. For this purpose, the discarded CPUs (Figure 6A), containing a large amount of metallic copper, nickel and gold, and so forth. (Figure 6B), are mechanically disassembled to obtain metal scraps, and further immersed into aqua regia to leach metals from CPUs. The resulting blue acidic leachate solution is tested to contain 1556 mg L^{-1} Cu(II), 234 mg L^{-1} Ni(II), 8.84 mg L^{-1} Fe(III), 1.24 mg L^{-1} Co(II), 1.03 mg L^{-1} Pb(II), 0.58 mg L^{-1} Cr(VI) together with 23.5 mg L^{-1} Au(III). In view of the extremely high acidity of aqua regia, the obtained CPU leachate is adjusted to pH 3.0 with KOH solution. In a typical experiment, 5 mg of the PIDO membranes are soaked in 100 ml of acidic CPU leachate, in which the concentrations of various metal ions in the tested leachate are determined by ICP-OES and the corresponding recovery efficiencies are calculated based on the content variation of each metal ion. As displayed in Figure 6C, the recovery efficiency of Au(III) on PIDO membrane reaches to over 99%; while the concentrations of other metal ions before and after treatment remain basically unchanged, indicative of the superior selectivity of PIDO membrane toward Au(III) from the leachate solution of e-waste despite the presence of interfering metal ions, especially Cu(II) and Ni(II) at rather

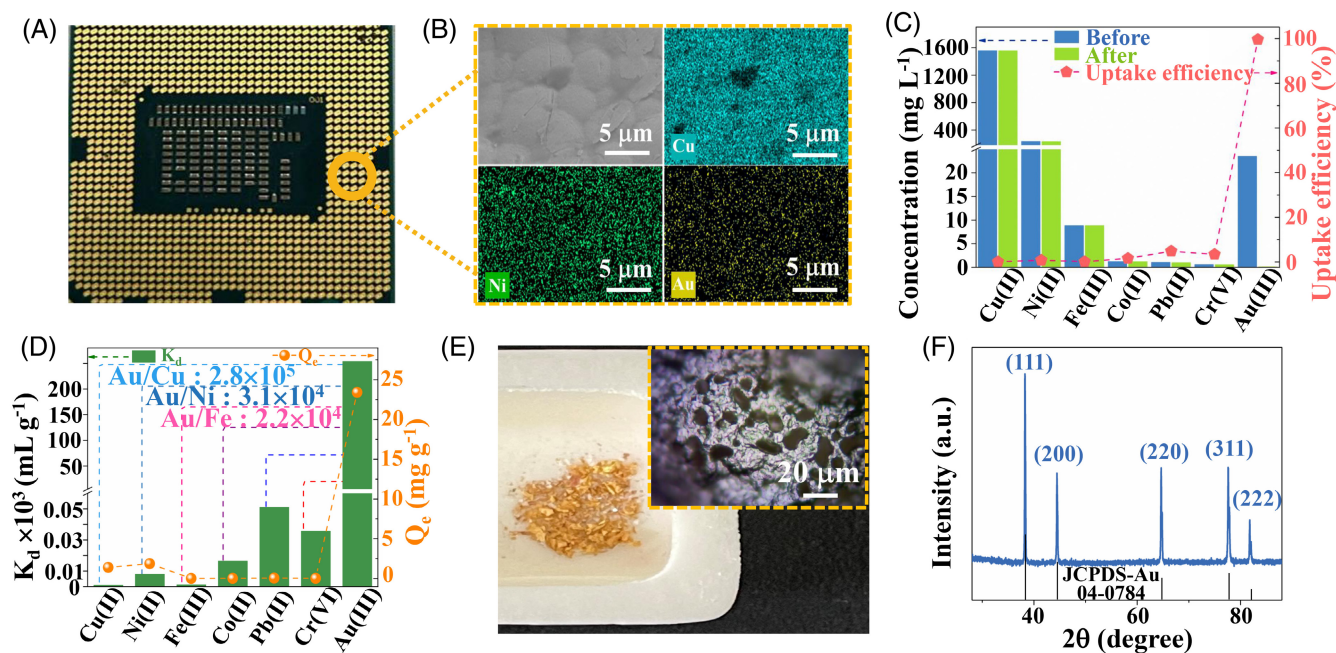


FIGURE 6 (A) Optical photograph and (B) Scanning electron microscopy image and Energy dispersive X-ray spectroscopy mappings of central processing unit (CPU). (C) The removal performance and (D) the affinity of various metal elements in CPU by poly(imine dioxime) (PIDO) membrane. (E) Optical photograph and microscope photograph of gold powder. (F) X-ray diffraction spectrum of gold powder

high concentrations. In order to reveal the recovery selectivity of PIDO membrane toward Au(III), the affinity of PIDO membrane to various metal ions is evaluated by the distribution coefficient (K_d). Generally speaking, an adsorbent with a K_d value $>10^4$ ml g^{-1} is regarded to possess excellent adsorption performance.³⁰ From Figure 6D, K_d values of Au(III), Cu(II), Ni(II), and Fe(III) are 2.6×10^5 , 0.9, 8, 1 ml g^{-1} , respectively. Evidently, K_d value of Au(III) is 4–5 orders of magnitude higher than other competitive metal ions. Further, the separation factor (SF) of A and B two ions ($SF_{A/B}$) is determined by K_d^A/K_d^B to quantify the adsorption preference, in which above 100 of separation factor signifies usually excellent separation degree.⁵⁵ In our case, the separation factor values for Au(III)/Cu(II), Au(III)/Ni(II), Au(III)/Fe(III), Au(III)/Co(II), Au(III)/Pb(II), and Au(III)/Cr(VI) are 2.8×10^5 , 3.1×10^4 , 2.2×10^4 , 1.5×10^4 , 5.0×10^3 , and 8.4×10^3 , respectively, highlighting the superior selectivity of PIDO membrane toward Au(III) over other coexisting metal ions. The phenomenon is well consistent with the corresponding hardness values of Cu(II), Ni(II), Fe(III), Co(II), Pb(II), Cr(VI) and Au(III) (0.55, 1.54, 2.6, 1.5, 0.93, 2.36, and 0.304, respectively).⁵⁶ Accordingly, as compared to base metals ions, soft Au(III) species possesses more preferable affinity toward N sites in amidoxime group based on the HSAB theory. More significantly, the distinctive gold species in form of $AuCl_4^-$ or $AuCl_3(OH)^-$ under acidic conditions are also responsible for their easy immobilization on the positively charged PIDO surface via electrostatic attraction; whereas other metal cations tend to be repulsed by the positively charged ADH@BC surface, accordingly generating low recovery efficiency.

Upon selective gold extraction from e-waste leachate, it is necessary to separate gold in elemental form from the PIDO membrane. To this end, the Au-loaded PIDO membranes are calcined at 1000°C in air for 5 h to decompose the organic constituents. Subsequently, metal powder pellets are collected and treated with concentrated hydrochloric acid to remove the unexpectedly physical adsorbed impurity. Under an optical microscope, the golden solid particles is observed (Figure 6E) and proved to be zero-valent metallic gold via XRD characterization (Figure 6F). It is noteworthy that there are no additional peaks from other metals or compounds, revealing high purity of the recycled gold from the e-waste leachate. Based on SEM observation (Figure S13a,b), the recovered gold particles are micron scale. From EDX spectrum (Figure S13c), no evidence of any other metals other than Au is found despite high concentrations of competing ions, such as Cu(II), Ni(II), etc., consistent with XRD results. To evaluate the metal contents and purity of the recovered gold,

the resulting solid powder is dissolved into aqua regia and subjected to subsequent elemental analysis via ICP-OES. As a consequence, the purity of the recovered gold pellets is identified to 23.6 karat, higher than those reported in most literatures.^{6,33} In order to more intuitively evaluate the economic feasibility of gold recovery from the CPU leaching solution, the production cost of PIDO membrane and the profit earned during gold recovery process are roughly calculated based on the price of the input raw materials, current gold price as well as the recovered gold amount using PIDO membrane. From the details supplied in Table S4, the cost of PIDO membrane is as low as \$0.097/g, far less than those for other gold adsorbents reported in the literature.^{1,33,57–61} More significantly, the generated gold income and profit/cost ratio for per gram PIDO membrane are \$584.4 and 6024.8, respectively, prevailing over other gold adsorbents by an overwhelming majority.^{1,33,57–61} In other words, the fabricated PIDO membrane possesses incomparable advantage in the economic benefits, thus ensuring cost-effective gold recovery from actual e-waste.

3 | CONCLUSION

To conclude, freestanding, hierarchically porous, hydrophilic, pure PIDO membranes can be massively fabricated via a simple evaporation-induced self-assembly technique based on the Marangoni effect. Thanks to abundant amidoxime binding sites, high specific surface area, ultrathin thickness, hierarchically porous characteristics, excellent hydrophilicity, and favorable mass transfer of adsorbates, the resulting PIDO membrane demonstrates excellent gold recovery performance, including record-breaking capacity, ultrafast kinetics, superior selectivity, outstanding regeneration and reusability. Furthermore, the real applicable feasibility of the fabricated PIDO membrane is exemplified in selectively and efficiently recovering gold from waste CPU leachate. The gold recovery mechanism is elucidated by XPS and DFT calculation, involving an energetically favorable adsorption/reduction process between cyclic imine dioxime and Au(III). In view of simple and fast processing, easy scaled-up production, low cost, mild condition, high reproducibility, and no need for expensive equipment, the current synthetic strategy fully meet the requirement for the large-scale economic extraction application of precious metals from real e-waste.

AUTHOR CONTRIBUTIONS

Huaimeng Li: Data collection, Writing - original draft, Investigation. **Mengxiang Ye:** Writing & editing.

Zhen Fu: Characterization and data analysis. **Haimin Zhang:** Reviewing and improving. **Guozhong Wang:** Project discussion. **Yunxia Zhang:** Funding acquisition, Writing - review & editing, Supervision.

ACKNOWLEDGMENTS

This work was financially supported by National Natural Science Foundation of China (Grant Nos. 52173268 and 51772299) and the Presidential Foundation of Hefei Institutes of Physical Science, Chinese Academy of Sciences (No. YZJJZX202019).

CONFLICT OF INTEREST

The authors declare no conflict of interest.

ORCID

Yunxia Zhang  <https://orcid.org/0000-0002-5312-6411>

REFERENCES

- Hong Y, Thirion D, Subramanian S, et al. Precious metal recovery from electronic waste by a porous porphyrin polymer. *Proc Natl Acad Sci USA*. 2020;117(28):16174-16180.
- Gurung M, Adhikari BB, Kawakita H, Ohto K, Inoue K, Alam S. Selective recovery of precious metals from acidic leach liquor of circuit boards of spent mobile phones using chemically modified persimmon tannin gel. *Ind Eng Chem Res*. 2012;51(37):11901-11913.
- Mon M, Ferrando-Soria J, Grancha T, et al. Selective gold recovery and catalysis in a highly flexible methionine-decorated metal-organic framework. *J Am Chem Soc*. 2016;138(25):7864-7867.
- Zeng X, Mathews JA, Li J. Urban mining of e-waste is becoming more cost-effective than virgin mining. *Environ Sci Technol*. 2018;52(8):4835-4841.
- Awasthi AK, Li J, Koh L, Ogunseitan OA. Circular economy and electronic waste. *Nat Electron*. 2019;2(7):86-89.
- Ma T, Zhao R, Li Z, et al. Efficient gold recovery from e-waste via a chelate-containing porous aromatic framework. *ACS Appl Mater Interfaces*. 2020;12(27):30474-30482.
- Sun D, Gasilova N, Yang S, et al. Rapid, selective extraction of trace amounts of gold from complex water mixtures with a metal-organic framework (MOF)/polymer composite. *J Am Chem Soc*. 2018;140(48):16697-16703.
- Aguila B, Sun Q, Cassidy HC, et al. A porous organic polymer nanotrapp for efficient extraction of palladium. *Angew Chem Int Ed*. 2020;59(1):19618-19622.
- Ji J, Bao Y, Liu X, Zhang J, Xing M. Molybdenum-based heterogeneous catalysts for the control of environmental pollutants. *EcoMat*. 2021;3(6):e12155.
- Xu X, Xu L, Ao J, et al. Ultrahigh and economical uranium extraction from seawater via interconnected open-pore architecture poly(amidoxime) fiber. *J Mater Chem A*. 2020;8(42):22032-22044.
- Shi S, Qian Y, Mei P, et al. Robust flexible poly(amidoxime) porous network membranes for highly efficient uranium extraction from seawater. *Nano Energy*. 2020;71:104629.
- Liu S, Wu M, Ye H, et al. Amidoximated cellulose microspheres synthesized via homogenous reactions for high-performance extraction of uranium from seawater. *Chem Eng J*. 2021;426:131378.
- Ma C, Gao J, Wang D, et al. Sunlight polymerization of poly (amidoxime) hydrogel membrane for enhanced uranium extraction from seawater. *Adv Sci*. 2019;6(13):1900085.
- Chen L, Bai Z, Zhu L, et al. Ultrafast and efficient extraction of uranium from seawater using an amidoxime appended metal-organic framework. *ACS Appl Mater Interfaces*. 2017;9(38):32446-32451.
- Zhao S, Yuan Y, Yu Q, et al. A dual-surface amidoximated halloysite nanotube for high-efficiency economical uranium extraction from seawater. *Angew Chem Int Ed*. 2019;131(42):15121-15127.
- Bai J, Ma X, Gong C, et al. A novel amidoxime functionalized porous resins for rapidly selective uranium uptake from solution. *J Mol Liq*. 2020;320:114443.
- Wang Y, Lin Z, Zhang H, et al. Anti-bacterial and super-hydrophilic bamboo charcoal with amidoxime modified for efficient and selective uranium extraction from seawater. *J Colloid Interface Sci*. 2021;598:455-463.
- Gao Q, Hu J, Li R, et al. Radiation synthesis of a new amidoximated UHMWPE fibrous adsorbent with high adsorption selectivity for uranium over vanadium in simulated seawater. *Radiat Phys Chem*. 2016;122:1-8.
- Xie S, Liu X, Zhang B, et al. Electrospun nanofibrous adsorbents for uranium extraction from seawater. *J Mater Chem A*. 2015;3(6):2552-2558.
- Yuan Y, Zhao S, Wen J, et al. Rational design of porous nanofiber adsorbent by blow-spinning with ultrahigh uranium recovery capacity from seawater. *Adv Funct Mater*. 2019;29(2):1805380.
- Liu T, Zhang R, Chen M, et al. Vertically aligned polyamidoxime/graphene oxide hybrid sheets' membrane for ultrafast and selective extraction of uranium from seawater. *Adv Funct Mater*. 2021;32(14):2111049.
- Yan B, Ma C, Gao J, Yuan Y, Wang N. An ion-crosslinked supramolecular hydrogel for ultrahigh and fast uranium recovery from seawater. *Adv Mater*. 2020;32(10):1906615.
- Yang F, Tao F, Li C, Gao L, Yang P. Self-assembled membrane composed of amyloid-like proteins for efficient size-selective molecular separation and dialysis. *Nat Commun*. 2018;9(1):5443.
- Chengara A, Nikolov AD, Wasan DT. Spreading of a water drop triggered by the surface tension gradient created by the localized addition of a surfactant. *Ind Eng Chem Res*. 2007;46(10):2987-2995.
- Wodlei F, Sebilliau J, Magnaudet J, Pimienta V. Marangoni-driven flower-like patterning of an evaporating drop spreading on a liquid substrate. *Nat Commun*. 2018;9(1):820.
- Wu X, Zhang J, Qin M, et al. ZnO electron transporting layer engineering realized over 20% efficiency and over 1.28 V open-circuit voltage in all-inorganic perovskite solar cells. *EcoMat*. 2022;e12192.
- Cheng Y, He P, Dong F, et al. Polyamine and amidoxime groups modified bifunctional polyacrylonitrile-based ion exchange fibers for highly efficient extraction of U(VI) from real uranium mine water. *Chem Eng J*. 2019;367:198-207.

28. Zhuang S, Wang J. Poly amidoxime functionalized carbon nanotube as an efficient adsorbent for removal of uranium from aqueous solution. *J Mol Liq.* 2020;319:114288.
29. Wang D, Song J, Wen J, et al. Significantly enhanced uranium extraction from seawater with mass produced fully amidoximated nanofiber adsorbent. *Adv Energy Mater.* 2018; 8(33):1802607.
30. Li H, Wang Y, Ye M, et al. Hierarchically porous poly (amidoxime)/bacterial cellulose composite aerogel for highly efficient scavenging of heavy metals. *J Colloid Interface Sci.* 2021;600:752-763.
31. Wang D, Song J, Lin S, et al. A marine-inspired hybrid sponge for highly efficient uranium extraction from seawater. *Adv Funct Mater.* 2019;29(32):1901009.
32. Astheimer L, Schenk HJ, Witte EG, Schwochau K. Development of sorbers for the recovery of uranium from seawater. Part 2. The accumulation of uranium from seawater by resins containing amidoxime and imidoxime functional groups. *Sep Sci Technol.* 1983;18(4):307-339.
33. Yang F, Yan Z, Zhao J, Miao S, Wang D, Yang P. Rapid capture of trace precious metals by amyloid-like protein membrane with high adsorption capacity and selectivity. *J Mater Chem A.* 2020;8(6):3438-3449.
34. Li H, Ye M, Zhang X, Zhang H, Wang G, Zhang Y. Hierarchical porous iron metal-organic gel/bacterial cellulose aerogel: ultra-fast, scalable, room-temperature aqueous synthesis, and efficient arsenate removal. *ACS Appl Mater Interfaces.* 2021;13(40): 47684-47695.
35. Xie D, Gu Y, Wang H, et al. Enhanced fluoride removal by hierarchically porous carbon foam monolith with high loading of UiO-66. *J Colloid Interface Sci.* 2019;542:269-280.
36. Zhang L, Zha X, Zhang G, et al. Designing a reductive hybrid membrane to selectively capture noble metallic ions during oil/water emulsion separation with further function enhancement. *J Mater Chem A.* 2018;6(22):10217-10225.
37. Setyawati MI, Xie J, Leong DT. Phage based green chemistry for gold ion reduction and gold retrieval. *ACS Appl Mater Interfaces.* 2014;6(2):910-917.
38. Park SI, Kwak IS, Won SW, Yun YS. Glutaraldehyde-crosslinked chitosan beads for sorptive separation of au(III) and Pd(II): opening a way to design reduction-coupled selectivity-tunable sorbents for separation of precious metals. *J Hazard Mater.* 2013;248:211-218.
39. Maruyama T, Matsushita H, Shimada Y, et al. Proteins and protein-rich biomass as environmentally friendly adsorbents selective for precious metal ions. *Environ Sci Technol.* 2007; 41(4):1359-1364.
40. Bolisetty S, Mezzenga R. Amyloid-carbon hybrid membranes for universal water purification. *Nat Nanotechnol.* 2016;11(4): 365-371.
41. Ishikawa S, Suyama K, Arihara K, Itoh M. Uptake and recovery of gold ions from electroplating wastes using eggshell membrane. *Bioresour Technol.* 2002;81(3):201-206.
42. Ji Y, Gao H, Sun J, Cai F. Experimental probation on the binding kinetics and thermodynamics of au(III) onto *Bacillus subtilis*. *Chem Eng J.* 2011;172(1):122-128.
43. Pethkar AV, Kulkarni SK, Paknikar KM. Comparative studies on metal biosorption by two strains of *Cladosporium cladosporioides*. *Bioresour Technol.* 2001;80(3):211-215.
44. Nguyen NV, Lee J, Kim S, Jha MK, Chung KS, Jeong J. Adsorption of gold(III) from waste rinse water of semiconductor manufacturing industries using Amberlite XAD-7HP resin. *Gold Bull.* 2010;43(3):200-208.
45. Wang Y, Gao X, Wu M, Tsubaki N. Thermocatalytic hydrogenation of CO₂ into aromatics by tailor-made catalysts: recent advancements and perspectives. *EcoMat.* 2021;3(1): e12080.
46. Shen G, Pan L, Zhang R, et al. Low-spin-state hematite with superior adsorption of anionic contaminations for water purification. *Adv Mater.* 2020;32(11):1905988.
47. Li J, Xu X, Liu W. Thiourea leaching gold and silver from the printed circuit boards of waste mobile phones. *Waste Manag.* 2012;32(6):1209-1212.
48. Zhang J, Ji Y, Wang P, Shao Q, Li Y, Huang X. Adsorbing and activating N₂ on heterogeneous au-Fe₃O₄ nanoparticles for N₂ fixation. *Adv Funct Mater.* 2020;30(4):1906579.
49. Li Y, Du Q, Liu T, et al. Methylene blue adsorption on graphene oxide/calcium alginate composites. *Carbohydr Polym.* 2013;95(1):501-507.
50. Dangi YR, Bediako JK, Lin X, et al. Polyethyleneimine impregnated alginate capsule as a high capacity sorbent for the recovery of monovalent and trivalent gold. *Sci Rep.* 2021; 11:17836.
51. Bai J, Chu J, Yin X, et al. Synthesis of amidoximated polyacrylonitrile nanoparticle/graphene composite hydrogel for selective uranium sorption from saline lake brine. *Chem Eng J.* 2020;391:123553.
52. Lin S, Reddy DHK, Bediako JK, et al. Effective adsorption of Pd(II), Pt(IV) and au(III) by Zr(IV)-based metal-organic frameworks from strongly acidic solutions. *J Mater Chem A.* 2017; 5(26):13557-13564.
53. Reddy KR, Maheswari CU, Venkateshwar M, Kantam ML. Selective oxidation of aromatic amines to nitro derivatives using potassium iodide-tert-butyl hydroperoxide catalytic system. *Adv Synth Catal.* 2009;351(1-2):93-96.
54. Das R, Sugimoto H, Fujii M, Giri PK. Quantitative understanding of charge-transfer-mediated Fe³⁺ sensing and fast photoresponse by N-doped graphene quantum dots decorated on plasmonic au nanoparticles. *ACS Appl Mater Interfaces.* 2020;12(4):4755-4768.
55. Sun Q, Aguila B, Earl LD, et al. Covalent organic frameworks as a decorating platform for utilization and affinity enhancement of chelating sites for radionuclide sequestration. *Adv Mater.* 2018;30(20):1705479.
56. Jolly WL. *Modern Inorganic Chemistry*. McGraw-Hill Companies; 2017.
57. Zhang L, Zheng Q, Xiao S, et al. Covalent organic frameworks constructed by flexible alkyl amines for efficient gold recovery from leaching solution of e-waste. *Chem Eng J.* 2021;426: 131865.
58. Chen Y, Li Z, Ding R, Liu T, Zhao H, Zhang X. Construction of porphyrin and viologen-linked cationic porous organic polymer

- for efficient and selective gold recovery. *J Hazard Mater.* 2022; 426:128073.
59. Liu J, Deng Z, Yu H, Wang L. Ferrocene-based metal-organic framework for highly efficient recovery of gold from WEEE. *Chem Eng J.* 2021;410:128360.
60. Zhang M, Dong Z, Hao F, et al. Ultrahigh and selective adsorption of au(III) by rich sulfur and nitrogen-bearing cellulose microspheres and their applications in gold recovery from gold slag leaching solution. *Sep Purif Technol.* 2021; 274:119016.
61. Zhang X, Li H, Ye M, Zhang H, Wang G, Zhang Y. Bacterial cellulose hybrid membrane grafted with high ratio of adipic dihydrazide for highly efficient and selective recovery of gold from e-waste. *Sep Purif Technol.* 2022;292:121021.

SUPPORTING INFORMATION

Additional supporting information can be found online in the Supporting Information section at the end of this article.

How to cite this article: Li H, Ye M, Fu Z, Zhang H, Wang G, Zhang Y. A freestanding, hierarchically porous poly(imine dioxime) membrane enabling selective gold recovery from e-waste with unprecedented capacity. *EcoMat.* 2022; 4(6):e12248. doi:[10.1002/eom2.12248](https://doi.org/10.1002/eom2.12248)